

Hartree-Fock Ground State Phase Diagram of Jellium

L. Baguet,¹ F. Delyon,² B. Bernu,¹ and M. Holzmann^{1,3}

¹LPTMC, UMR 7600 of CNRS, Université P. et M. Curie, Paris, France

²CPHT, UMR 7644 of CNRS, École Polytechnique, Palaiseau, France

³Univ. Grenoble 1/CNRS, LPMCM UMR 5493, Maison des Magistères, 38042 Grenoble, France

(Dated: July 12, 2013)

We calculate the ground state phase diagram of the homogeneous electron gas in three dimensions within the Hartree-Fock approximation and show that broken symmetry states are energetically favored at any density against the homogeneous Fermi gas state with isotropic Fermi surface. At high density, we find metallic solutions where electronic charge and spin density form an incommensurate crystal having more crystal sites than electrons, whereas the commensurate Wigner crystal is favored at lower densities, $r_s \gtrsim 3.4$. Decreasing the density, the system undergoes several structural phase transitions with different lattice symmetries, changing from spin unpolarized to fully polarized Wigner crystals at $r_s \gtrsim 8.5$.

PACS numbers: 71.10.-w, 71.10.Ca, 71.10.Hf, 71.30.+h, 03.67.Ac

The understanding of electrons in solid state and condensed matter has been one of the major challenges since the discovery of quantum mechanics. The simplest model system representing condensed matter is the homogeneous electron gas (jellium) where electrons interact with each other and with a uniform positive charged background density $3/(4\pi r_s^3)a.u.$ instead of the nuclei. For almost one century, jellium has been the central model for qualitative and quantitative studies of electronic correlation¹⁻¹⁰.

The Hartree-Fock approximation (HF) plays an absolutely fundamental role in tackling many-body electron problems. As the best possible description within the independent particle approximation, it provides both, reference and starting point, for any more sophisticated calculations. However, even though the HF ground state of jellium has been subject of research all over the years¹⁰⁻¹², the ground state phase diagram as a function of the density has still not fully been established. At low density, potential energy largely dominates over the kinetic energy, and the electrons form the so-called Wigner crystal (WC), the ground state in the classical limit, whereas in the limit of vanishing r_s the ideal Fermi gas (FG) is approached. Overhauser has argued that the FG solution never represents the true HF ground state at any finite density¹⁰. Only quite recently, indications for a ground state with broken spin symmetry in the high density region were found in explicit numerical calculations for small and moderate sizes¹². However, its energy gain compared to FG has not been established in the thermodynamic limit.

Here, we present the Hartree-Fock phase diagram covering relevant crystal structures¹³. Generalizing previous approaches to form charge/spin-broken symmetry states^{10,12}, our study also includes the possibility of incommensurate crystals of charge/spin-density. In contrast to WC states, the number of maxima of the charge/spin density there differs from the number of electrons, thus providing broken symmetry states with metallic character^{14,15}. At high densities, we find that these

incommensurate states are favored against FG and WC. Our method allows us to treat large enough systems to obtain results valid in thermodynamic limit, necessary to clearly establish the tiny gain of energy for these states. Our study also suggest new candidate ground states for jellium and jellium-like systems¹⁶, that should be explored by more accurate many-body approaches^{1,9}.

We consider a system of N electrons in a volume V , embedded in an homogeneous background of opposite charge, interacting through the Coulomb potential. Hartree-Fock solutions are Slater determinants $|\Psi\rangle = \bigwedge_{\alpha \in S} |\phi_\alpha\rangle$ constituted by a set S of single-particle states ϕ_α . In terms of density matrix, the Hartree-Fock solutions can be defined by a 1-body density matrix ρ_1 such that $\text{Tr } \rho_1 = 1$ and $0 \leq \rho_1 \leq 1/N$. The two-body density matrix ρ_2 satisfies:

$$\rho_2(\underline{1}, \underline{2}; \underline{1}', \underline{2}') = \rho_1(\underline{1}; \underline{1}')\rho_1(\underline{2}; \underline{2}') - \rho_1(\underline{1}; \underline{2}')\rho_1(\underline{2}; \underline{1}'). \quad (1)$$

Now we restrict our study to periodic states:

$$(\rho_1 \psi)(\mathbf{k} + \mathbf{q}, \sigma) = \sum_{\mathbf{q}' \in \Lambda, \sigma'} \rho_{\mathbf{k}}(\mathbf{q}, \sigma; \mathbf{q}', \sigma') \psi(\mathbf{k} + \mathbf{q}', \sigma') \quad (2)$$

with $\mathbf{k} \in \mathcal{B}$, $\mathbf{q} \in \Lambda$, where \mathcal{B} is the Brillouin zone of a lattice Λ , generated by \mathbf{Q}_1 , \mathbf{Q}_2 , and \mathbf{Q}_3 , and $\rho_{\mathbf{k}}$ are positive matrices satisfying $0 \leq \rho_{\mathbf{k}} \leq 1/N$. The direct space lattice is defined by $\mathbf{L}_i \cdot \mathbf{Q}_j = 2\pi\delta_{ij}$, and our periodic simulation box is a parallelepiped of sizes $M\mathbf{L}_i$, for some integer M , and volume $V \sim M^3$.

We have checked on a few cases that the best solutions are either fully polarized or unpolarized, thus, in the following, we impose $\rho_{\mathbf{k}}(\mathbf{q}, \sigma; \mathbf{q}', \sigma') = \rho_{\mathbf{k}, \sigma}(\mathbf{q}; \mathbf{q}')\delta_{\sigma, \sigma'}$. Without any specification, $k_F = (6\pi^2 N/(n_s V))^{1/3}$ denotes the Fermi wave vector according to the polarization of the corresponding state, with $n_s = 2$ (resp. 1) for the unpolarized gas (U) (resp. polarized (P)). For FG solutions, we have $\rho_{\mathbf{k}, \sigma}(\mathbf{q}, \mathbf{q}') = \delta_{\mathbf{q}, \mathbf{q}'} \Theta(k_F - \|\mathbf{k} + \mathbf{q}\|)/N$ with energy $E_{FG} = 3\alpha^2/(10r_s^2) - 3\alpha/(4\pi r_s)$, where $\alpha = [9\pi/(2n_s)]^{1/3}$.

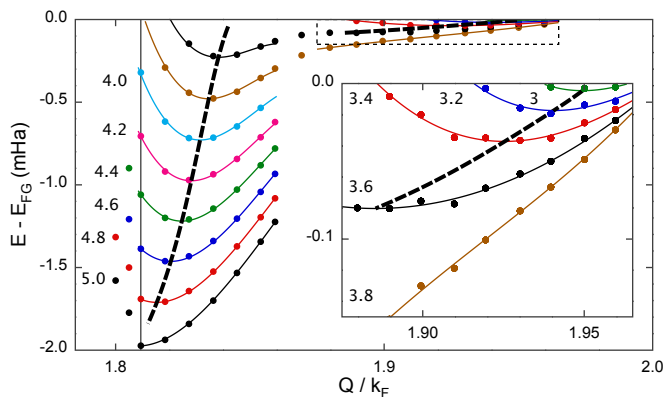


FIG. 1. Energy versus the modulation Q at various r_s for the unpolarized gas in the bcc symmetry. Lines comes from a global polynomial fit on the numerical results (circles) of order 2 and 3 in r_s and Q , respectively. r_s is indicated at the start of each curve. Thick dashed lines go through the local minima. The leftmost vertical straight line stands for $Q = Q_W$. Inset: zoom of the dotted rectangle of the main figure.

On the other hand, in the Wigner crystal, each $\rho_{\mathbf{k}}$ is $1/N$ times a projector of rank n_s . This case has already been considered with various symmetries in Ref.¹¹, but their solutions did not lower the energy for $r_s \leq 4.4$ and a transition to the FG has been predicted.

Of course, the true ground state solutions are expected to be somewhere between the FG and WC solutions. Unrestricted HF calculations for small systems¹² ($N < 10^3$) have indicated the possibility of a spin-density wave in this region with energy gains of order 10^{-4} Ha with respect to FG. In fact, at small r_s , as the system goes to the FG, the crystalline order remains but the Brillouin zone becomes partially occupied. In particular, the number of particles per unit cell is not known a priori. The purpose of this paper is to find these extremal periodic states without extra hypotheses for various lattice symmetries.

Thus, we search for a lattice Λ and a density matrix $\rho_{\mathbf{k}}$ such that the number of particles per unit cell is near n_s (or some multiple of n_s for non-Bravais lattices (nBL)). Notice that for extremal states, the eigenvalues of $\rho_{\mathbf{k}}$ must be exactly 0 or $1/N$. The number of strictly positive eigenvalues is not known a priori, but is expected to fall between 0 and $2n_s$ (or some multiple of $2n_s$ for nBL).

We truncate the number of vectors of the sub-lattice Λ , including only the first M_Λ bands: $\rho_{\mathbf{k}}$ is a square matrix of order $n_s M_\Lambda$. The condition $0 \leq \rho_{\mathbf{k}} \leq 1/N$, is difficult to fulfill. So we choose the representation:

$$\rho_{\mathbf{k}} = \sum_i D_{\mathbf{k},i} |u_{\mathbf{k},i}\rangle \langle u_{\mathbf{k},i}| \quad (3)$$

where $\langle u_{\mathbf{k},i} | u_{\mathbf{k},j} \rangle = \delta_{ij}$ and $0 \leq D_{\mathbf{k},i} \leq 1/N$. Since the number of strictly positive $D_{\mathbf{k},i}$ is between 0 and $2n_s$, we can restrict the summation in Eq. (3) over $2n_s$ terms instead of $n_s M_\Lambda$. The number of unknowns is thus of

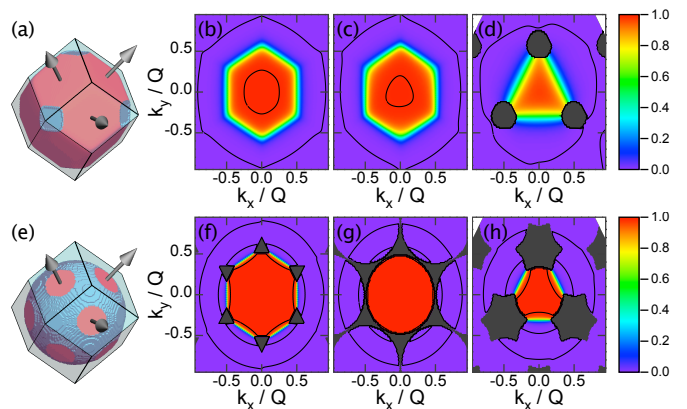


FIG. 2. Momentum distribution per spin $n(\mathbf{k})$ for incommensurate solutions in bcc symmetry. Figure (a) is an isosurface at $n(\mathbf{k}) = 0.5$ for $Q/k_F \approx 1.827$, $r_s = 4.2$, $M = 64$ and $M_\Lambda = 19$. The jump of $n(\mathbf{k})$ from 0 to a non-zero value are shown in blue. Black arrows stands for reciprocal lattice vectors ($\mathbf{Q}_1, \mathbf{Q}_2, \mathbf{Q}_3$). On (b), (c), and (d) : cut of $n(\mathbf{k})$ at $k_1 = 0$, $k_1 = Q/4$, and $k_1 = Q/2$ respectively. Black areas correspond to $n(\mathbf{k}) = 0$. Contour levels are at 0.1 , 10^{-3} and 10^{-5} . (e-h): same as (a-d) for $Q/k_F \approx 1.940$ and $r_s = 3.2$.

order $2n_s M_\Lambda$ times the number of vectors of \mathcal{B} . This is why we can deal with large number of particles¹⁷.

The minimization consists in the following steps. At first we choose $D_{\mathbf{k},i}$ and $|u_{\mathbf{k},i}\rangle$ to start with. Then, for $D_{\mathbf{k},i}$ fixed, we find the best $|u_{\mathbf{k},i}\rangle$ with a quadratic descent method¹⁴. The next step is to try to improve $D_{\mathbf{k},i}$ given the gradient of the energy with respect to $D_{\mathbf{k},i}$ and the linear constraints, $0 \leq D_{\mathbf{k},i} \leq 1/N$ and $\sum_{\mathbf{k},i} D_{\mathbf{k},i} = 1$. We thus obtain a new set $D_{\mathbf{k},i}^{(\text{new})}$ (either 0 or $1/N$), and we change $D_{\mathbf{k},i}$ into $(1 - \varepsilon)D_{\mathbf{k},i} + \varepsilon D_{\mathbf{k},i}^{(\text{new})}$ (with a small enough ε to ensure that $|u_{\mathbf{k},i}\rangle$ follows $D_{\mathbf{k},i}$ adiabatically) and we restart the minimization with respect to $|u_{\mathbf{k},i}\rangle$. The process stops as soon as $D_{\mathbf{k},i}^{(\text{new})} = D_{\mathbf{k},i}$. In this case almost every $D_{\mathbf{k},i}$ are 0 or $1/N$ and the gradient is negative or positive accordingly.

The parameters are r_s (for the density), the lattice symmetry, the (smallest) modulus Q of the generators of Λ , the number M^3 of points in the Brillouin zone \mathcal{B} and the number M_Λ of plane waves per single-particle state.

A priori, we look for lattices with the lowest Madelung energies as they will lead to the more stable states at low densities. However, as the density increases, other lattices may become more favorable. Investigated lattices are: simple cubic (sc), face-centered cubic (fcc), body centered cubic (bcc) and hexagonal (Hex) (see Table I).

For WC phases, $Q = Q_W$, whereas $Q \neq Q_W$ characterizes incommensurate crystals, and $Q \geq 2k_F$ leads to the FG solution with isotropic Fermi surface at k_F . Increasing M_Λ increases the basis resulting in a lower energy due to the variational principle. Our discretization of the Brillouin zone ranges from $M = 32$ up to $M = 128$ which corresponds to effective system sizes with number

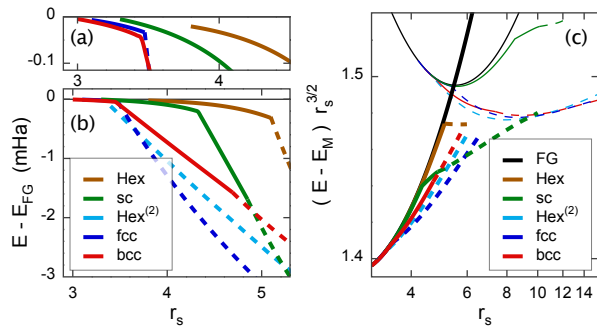


FIG. 3. Phase diagram of the electron gas: unpolarized (a) and (b), polarized and unpolarized (c). Energies are in milli-Hartrees for (a) and (b), and in Hartrees for (c), where $E_M = 0.89593/r_s$ is the Madelung energy of a polarized-bcc Wigner crystal. Full lines stand for incommensurate regime ($Q > Q_W$) and dashed lines for the Wigner crystal ($Q = Q_W$). Colors refer to the lattice (see Table I). (a): zoom of (b) around $E - E_{FG} = 0$. (c): thin lines stand for the polarized gas (upper curves) and thick lines for the unpolarized gas¹³.

Unpolarized					
Symmetry	IC-bcc	Hex ⁽²⁾ (hcp*)	fcc	sc	Hex
n_m	2	4	2	2	2
Charge	IC-bcc ⁽²⁾	Hex ⁽⁴⁾	sc	bcc	hcp
T	$(\frac{1}{2}, \frac{1}{4}, 0)$	T_2	$(\frac{1}{2}, 0, 0)$	$(\frac{1}{2}, \frac{1}{2}, \frac{1}{2})$	T_1
r_s	3 – 3.4	3.4 – 3.7	3.7 – 5.9	5.9 – 9.3	
Polarized					
Symmetry	sc	Hex ⁽²⁾ (hcp)	fcc	bcc	
n_m	1	2	1	1	
r_s		9.3 – 10.3	10.3 – 13	13 –	

TABLE I. The best overall ground states depending on r_s (last line). (IC) stands for incommensurate crystal, otherwise it is WC. n_m is the number of maxima of charge density per unit cell¹⁹. T is the shift between the spin up and down lattices, in the conventional (cartesian) cell basis for sc, fcc and bcc lattices, and in the primitive cell basis for Hex and Hex⁽²⁾ (number in parenthesis is the number of sites per cell). $T_1 = (\frac{1}{3}, \frac{2}{3}, \frac{1}{2})$, $T_2 = (\frac{1}{2}, 0, \frac{1}{4})$. The star means close to. The last line of each table indicates the range of r_s where each phase may be in the ground state.

of electrons ($\sim M^3$) much larger than those of Ref.¹².

Finite size effects are important in fermionic Coulomb systems¹⁸ and, contrary to M_Λ , there is no variational principle. As the memory size increases $\propto M_\Lambda^2 M^3$, pure numerical extrapolation to the thermodynamic limit ($M \rightarrow \infty$) is difficult. Therefore, to accelerate convergence, we have included finite size corrections:

$$\Delta E_M \equiv E_M - E_\infty = E_M^{(1)} + E_M^{(2)} + E_{NA} \quad (4)$$

where $E_M^{(1)} \sim 1/M$ is the analytically known Madelung energy, $E_M^{(2)}$ is an analytical error of order $1/M^2$, and E_{NA} a non analytical term of order $1/M^3$. Both, $E_M^{(1)}$ and $E_M^{(2)}$, arise from a potential energy error, whereas

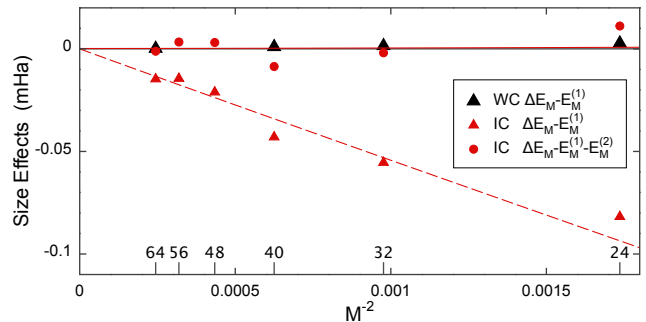


FIG. 4. Size effects on the potential energy for the U-bcc lattice, Eqs. (4-5). $E_M^{(i)}$ is the correction of order $1/M^i$. In red and black are the data for IC [$r_s = 3.4, Q/k_F = 1.92$] and WC [$r_s = 5$], respectively. Red circles include second order correction for IC ($E_M^{(2)} = 0$ for WC). The red dashed (resp. full) line is a fit of the form $E_M^{(2)} + b/M^3$ (resp. b/M^3). Numbers at the bottom indicate M .

E_{NA} contains also kinetic energy contributions. From the FG-potential energy, $E_M^{(2)}$ can be estimated as:

$$E_M^{(2)} = - \left(\frac{\gamma}{\pi M} \frac{S(\mathbf{k})}{\|\mathbf{k}\|} \Big|_{k \rightarrow 0} \right) \times E_M^{(1)} \quad (5)$$

where γ^3 is the volume of \mathcal{B} , and $S(\mathbf{k})$ is the structure factor (for FG, $\lim_{k \rightarrow 0} S(\mathbf{k})/\|\mathbf{k}\| = 3/(4k_F)$). Notice that $E_M^{(2)}$ is maximum for FG, decreases with Q for incommensurate solutions, and vanishes for WC. As can be seen in Fig.4, removing $E_M^{(2)}$ greatly improves the thermodynamic limit extrapolation. Note, however, that non-analytical contributions are still visible for our system sizes. Indeed, they become important at high density and prevent a precise extrapolation for $r_s \lesssim 3$.

The accuracy of the results is essentially controlled at large r_s by M_Λ ($\rho_{\mathbf{k}}$ smooth but extended) and at small r_s by M ($\rho_{\mathbf{k}}$ rapidly varying around k_F). Fig.(1) shows the energy differences $\Delta E = E - E_{FG}$ versus the modulation Q at various r_s for the U-bcc symmetry. At large r_s , the minimum is found for $Q = Q_W$. At smaller r_s , a minimum is eventually reached for $Q > Q_W$. As seen in Fig. (1), two local minima may occur. Furthermore, at the local minima, the best solutions are always found with only one band (i.e., for each $\mathbf{k} \in \mathcal{B}$ in Eq. (3), at most one $D_{\mathbf{k},i}$ is non-zero).

The momentum distribution $n(\mathbf{k})$ shows how the incommensurate states interpolate between the Wigner phase, $Q = Q_W$, and the Fermi gas ($Q = 2k_F$). For WC, the first band in \mathcal{B} is fully occupied and $n(\mathbf{k})$ is everywhere continuous. At $Q \gtrsim Q_W$, the first band becomes partially filled and unoccupied volumes appear around the corners of \mathcal{B} (see Fig 2-a,d), leading to a possible minimum at some Q_{\min} . Thus $n(\mathbf{k})$ is discontinuous at the surface of these volumes but stay continuous in other directions. As Q increases, the volumes connect allowing an eventual second minimum at $Q \lesssim 2k_F$ (see Fig 2-e-g).

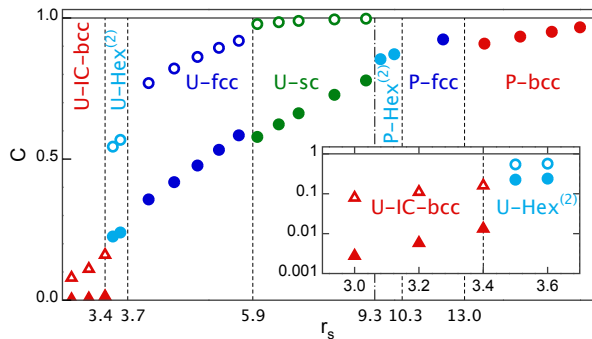


FIG. 5. Contrast C of $n(\mathbf{r})$ versus r_s for the ground states. Full symbols: charge density. Open symbols (for unpolarized gas): spin up (or down) density. Circle: Wigner Crystal. Triangle: Incommensurate phase (IC). Inset: zoom of the low- r_s part. Vertical lines separate the different unpolarized (U) and polarized (P) phases.

At $Q = 2k_F$, the Fermi sphere is completed, where $n(\mathbf{k})$ is discontinuous at the Fermi surface.

By construction, the real-space density, $n(\mathbf{r})$, has the crystalline symmetry of the lattice. In the incommensurate phase (IC), the number of maxima is greater than the number of electrons and depends on Q . At large r_s , the numbers coincide, this is the Wigner crystal. We define a contrast by $C = (n^{\max} - n^{\min}) / (n^{\max} + n^{\min})$ which goes from 0 to 1 as r_s goes from 0 to infinity, where n^{\max} and n^{\min} are the maxima and minima of $n(\mathbf{r})$. For the unpolarized gas, we define the contrast for each spin-species and for the total charge. As shown in Fig. (5), the contrast decreases rapidly as r_s goes to zero; it is expected²⁰ to be a non-analytic function at $r_s = 0$. Notice that the charge density modulation is much smaller

than each spin modulation in the unpolarized gas.

The final phase diagram with all phases is reported in Fig.3. As the energy differences from the FG vary strongly with r_s , two representations are used: $E - E_{FG}$ for r_s around the transitions from WC to IC in Fig.3-a-b, and a representation where all energies are similar in the range of interest in Fig.3-c. Various phases are found in both polarization depending on the value of r_s (see Table I). Extending the analytical calculations of Ref.²⁰ from two to three dimensions, one can prove that the incommensurate phases are always energetically favorable for $r_s \rightarrow 0$. However, our numerical precision is insufficient to clearly determine the symmetry for $r_s < 3$ as the energy differences between the phases become comparable to the remaining error in the size extrapolation.

To conclude, we have established the true ground state phases of jellium within Hartree-Fock over a broad density region. We find explicit HF wave functions, with $u_{\mathbf{k},i} > 0$ (modulo a global translation factor). In particular, we have shown that the Overhauser instability¹⁰ of the FG results in a new ground state in the thermodynamic limit, characterized by an incommensurate crystal structure for the spin and charge density. However, it is known that Hartree Fock tends to favor crystalline phases, as the gain in correlation energy is typically higher in the isotropic FG phase than in the WC¹. Therefore, the transition to the WC is quantitatively incorrect within HF and shifted towards considerable higher values of r_s in the true ground state phase diagram. Whereas correlations certainly stabilize the FG at small r_s , correlations should favor incommensurate phases compared to WC for the same reason, so that incommensurate states should actually occur at densities close to crystallization. We hope that future QMC calculations will be able to establish this new phase beyond HF.

¹ D. M. Ceperley and B. J. Alder, Phys. Rev. Lett. **45**, 566-569 (1980).
² B. Tanatar and D.M. Ceperley, Phys. Rev. B **39**, 5005 (1989).
³ G. F. Giuliani and G. Vignale, *Quantum Theory of the Electron Liquid*, Cambridge University Press, Cambridge (2005).
⁴ E. P. Wigner, Trans. Faraday Soc. **34**, 678 (1938); Phys. Rev. **46**, 1002 (1934).
⁵ B. Bernu, L. Candido, D. Ceperley Phys. Rev. Lett. **86**, 870 (2001).
⁶ L. Cândido, B. Bernu, and D.M. Ceperley, Phys. Rev. B **70**, 094413 (2004).
⁷ M. Holzmann, B. Bernu, V. Olevano, R. M. Martin, and D. M. Ceperley, Phys. Rev. B **79**, 041308 (2009).
⁸ M. Holzmann, B. Bernu, C. Pierleoni, J. McMinis, D.M. Ceperley, V. Olevano, and L. Delle Site, Phys. Rev. Lett. **107**, 110402 (2011).
⁹ J. J. Shepherd, G. Booth, A. Grneis, and A. Alavi, Phys. Rev. B **85**, 081103(R) (2012).
¹⁰ A. W. Overhauser, Phys. Rev. Lett. **4**, 462 (1960); Phys.

Rev. **128**, 1437 (1962).
¹¹ J. R. Trail, M. D. Towler, and R. J. Needs, Phys. Rev. B **68**, 045107 (2003).
¹² S. Zhang and D. M. Ceperley, Phys. Rev. Lett. **100**, 236404 (2008), arXiv:0712.1194 (2007).
¹³ When comparisons are possible, our energies are always lower than Ref.¹¹, despite the size effects which increase energies versus r_s .
¹⁴ B. Bernu, F. Delyon, M. Duneau, and M. Holzmann, Phys. Rev. B **78**, 245110 (2008).
¹⁵ B. Bernu, F. Delyon, M. Holzmann and L. Baguet, Phys. Rev. B **84**, 115115 (2011).
¹⁶ S. Huotari, J. A. Soininen, T. Pykkänen, K. Hämäläinen, A. Issolah, A. Titov, J. McMinis, J. Kim, K. Esler, D. M. Ceperley, M. Holzmann, and V. Olevano, Phys. Rev. Lett. **105**, 086403 (2010).
¹⁷ This method needs less space memory and CPU times than that of ref.¹⁵
¹⁸ S. Chiesa, D.M. Ceperley, R.M. Martin, and M. Holzmann, Phys. Rev. Lett. **97**, 076404 (2006).

¹⁹ For Wigner solutions, n_m is also the number of electrons per unit cell.

²⁰ F. Delyon, M. Duneau, B. Bernu, and M. Holzmann, *cond-mat/0807.0770*.